Nonlinear Dynamics of the Wake of an Oscillating Cylinder

D. J. Olinger and K. R. Sreenivasan

Mason Laboratory, Yale University, New Haven, Connecticut 06520

The wake of an oscillating cylinder at low Reynolds numbers is a nonlinear system in which a limit cycle due to natural vortex shedding is modulated, generating in phase space a flow on a torus. We experimentally show that the system displays Arnol'd tongues for rational frequency ratios, and approximates the devil's staircase along the critical line. The "singularity spectrum" as well as spectral peaks at various Fibonacci sequences accompanying quasiperiodic transition to chaos show's that the system belongs to the same universality class as the sine circle map.

In low-dimensional dynamical systems, detailed predictions have been made for the "universal" features of transition to chaos by period-doubling[1,2] and quasiperiodic[3-6] routes. Experiments in small–aspect-ratio closed-flow systems[7-9] have gone a long way in establishing the validity of these predictions to fluid flows. However, experiments in open-flow systems (those with imposed unidirectional main flow) with little or no confinement have paid heed to these predictions only rarely.[10-13] The best case for showing some conformity with features of nonlinear dynamics is the flow behind circular cylinders.[10,13] Here, we study at low Reynolds numbers the flow behind a circular cylinder oscillating transverse to an oncoming stream, and show that it exhibits some quantitative features of universality.

Briefly, with increasing Reynolds number, the flow behind a stationary cylinder first undergoes a Hopf bifurcation[14] from the steady state to a periodic state characterized by the vortex-shedding mode at a frequency f_0, say. We have shown in Ref. 14 that the post-critical state can be modeled by the Landau equation, and determined the Landau constants. For cylinder aspect ratio (that is, the length to diameter ratio) exceeding about 60, details of this bifurcation are independent of the aspect ratio, and the critical Reynolds number (based on the cylinder diameter D and the oncoming velocity) is about 46. For the present measurements, the working fluid was air, and the Reynolds number about 55. A modulation was imposed by our causing the cylinder to oscillate transverse to the main flow at a frequency f_e, the amplitude of oscillation being then a measure of the nonlinear coupling between the two modes. The system has two competing frequencies (f_0 and f_e) yielding two control parameters, f_e/f_0 and the nondimensional amplitude of oscillation, a/D. Once the external modulation is imposed, we expect f_0 to shift to f_0', say. This is similar in spirit to the convection experiments of Refs. 7 and 8, and the well-studied sine circle map.

$$\theta_{n+1} = \theta_n + \Omega - (K/2\pi)\sin(2\pi\theta_n),$$

for which Ω is the bare winding number (equal to the average shift per iteration in the absence of nonlinear coupling—analogous to f_e/f_0), and K is the nonlinearity parameter, comparable to a/D. The average shift per iteration in the presence of nonlinear coupling is the dressed winding number, ω, comparable to f_e/f_0'. The sine circle map has been studied in recent years as a standard model for the transition from quasiperiodicity to chaos in dynamical systems, and its properties are believed to be universal for any map with a cubic inflection point. For $K < 1$ (subcritical behavior), iterates of the map lock on to rational ω values (in general different from Ω for nonzero amplitudes of oscillation) in the Arnol'd tongues[15] which increase in width as K increases. At $K = 1$, the critical line, a universal transition to chaos occurs at a special value of the dressed winding number, $\sigma_G = (\sqrt{5} - 1)/2$, the inverse of the golden mean. To observe the universal transition to chaos, it is best to move without phase locking along the line $\omega = \sigma_G$ up to the critical point, this choice being relevant because the irrational number σ_G is least well approximated by rationals (containing only ones in the continued-fraction representation). The universal behavior at the critical golden-mean point is observed in the scaled power spectrum and in the self-similar devil's staircase structure along the critical line,[3-7] and the so-called $f(\alpha)$ curve.[16]

Our motivation for studying the oscillating cylinder within this framework is twofold. First, there is evidence[17] of lock-in when f_e is near f_0 (Ω near 1). Our search for additional phase-locked tongues at other rational ω's constitutes a generalization of this work within the framework of dynamical systems. Second, analogies can be drawn between our flow and other fluid systems (most notably the forced Rayleigh-Bénard system) which have exhibited quantitative experimental results reminiscent of sine circle maps. Establishing this fact in a different, and by all accounts more complex, fluid system has broad implications transcending the immediate measurements.

The cylinder was placed in a wind tunnel of the suction type with double contractions, honeycomb, and
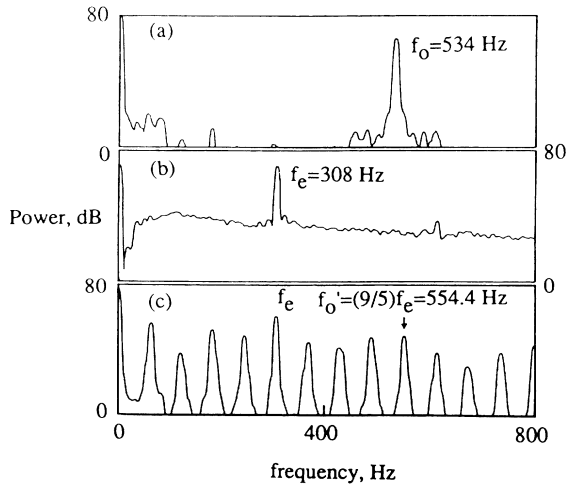
FIG. 1. (a) Power spectral density for the case of natural vortex shedding at $f_0 = 534$ Hz. (b) The corresponding data for the excitation source, measured with a photodiode; $f_e = 308$ Hz. (c) Frequency locking occurring as a result of excitation. The natural shedding frequency disappears in favor of the new peak at $\frac{9}{5} f_e$; peaks appear at other fractions of f_e.

several damping screens, and was made to oscillate at the desired frequency by the passage of a sinusoidally alternating current through it in the presence of a properly aligned magnetic field. Both the vortex-shedding and modulation frequencies were steady to ± 2 parts in 10^4. A hot wire, 5 μm in diameter and 0.6 mm in length, placed approximately $15D$ downstream of the cylinder, $0.5D$ to one side of its mean position, monitored the flow velocity. The hot-wire signal was amplified, digitized by a twelve-bit analog-to-digital converter, and stored in a computer (MASSCOMP 5500) for later analysis. A HP3561A spectrum analyzer was used for real-time analysis. The cylinder oscillation frequency and amplitude were varied over a range of (26–100)% of f_0 and (0–200)% of the cylinder diameter. The cylinder diameter varied from 0.03 to 0.09 cm, and its active length was 15 cm; the actual length of the cylinder, stretching outside the wind tunnel, was about 3 times as long. The cylinder always oscillated in its first mode.

Figure 1 highlights the effect of cylinder oscillations on the wake-velocity power spectrum. We note the shift of f_0 to f_0' between Figs. 1(a) and 1(c), and the complete suppression of f_0 in favor of f_0' in Fig. 1(c). All the principal peaks in Fig. 1(c) (linear combinations of f_e and f_0') are more than 5 orders of magnitude above background noise levels. From several such spectra, one can plot a "phase" diagram showing Arnol'd tongues (Fig. 2). All symbols represent boundaries of the larger tongues shown. The exception is the triangle symbol, which represents the $\frac{5}{9}$ lock-in shown in detail in Fig. 1. The dressed winding numbers in these tongues correspond to rationals constructed according to Farey arithmetic although, because of limitations in experimental
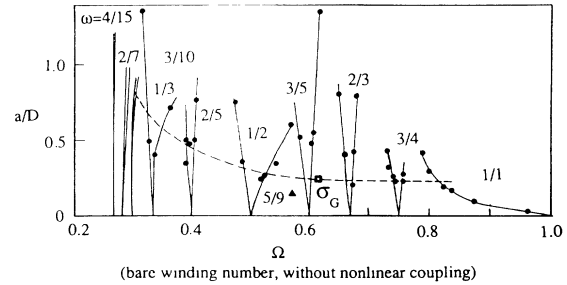

(bare winding number, without nonlinear coupling)

FIG. 2. Arnol'd tongues (that is, the locked-in regions) in the wake of the oscillating cylinder. The ordinate is the amplitude of oscillation normalized by the cylinder diameter. About 30 such tongues were noted, but only those with reasonable width are shown. In each tongue, the natural shedding frequency disappears in favor of a rational multiple of the excitation frequency, and the appropriate multiplication factor is shown in each tongue. The critical line (corresponding to the $K = 1$ line in the circle map), as determined by the expected fractal dimension, is shown dashed.

control, no more than 30 such tongues have been identified. (To avoid cluttering, not all of them are shown.) In accordance with predictions for the circle map, these tongues increase in width as a/D increases. The 1/1 tongue is in close agreement with the previously mentioned lock-in region near f_0. The dashed line represents the experimentally determined "best fit" critical line found by our determining, for various Ω, the a/D level at which the fractal dimension D_0 of the critical line was equal to 0.87 appropriate to the circle map. The dimension D_0 was computed with

$$\sum (S_i/S)^{D_0} = 1,$$

where S is the distance between two parent tongues around an irrational winding number and the S_i's ($i = 1,2$) are the distances between a daughter tongue, constructed according to Farey arithmetic, and each of its parents. All possible parent-daughter combinations of tongues shown in Figs. 2 and 3 were used. A few measurements on the onset of chaos at different Ω yield-
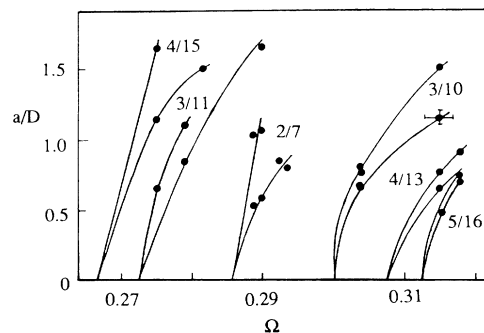

FIG. 3. The fine structure in a small region of the $(a/D, \Omega)$ plane of Fig. 2. Typical experimental uncertainties are shown.
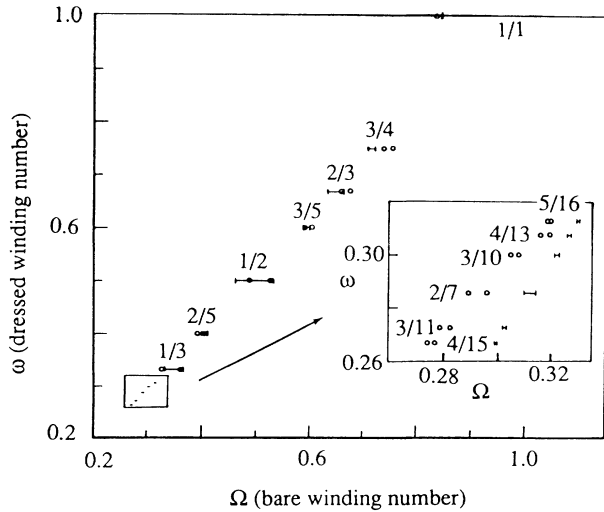
FIG. 4. The devil's-staircase construction with the data of Figs. 2 and 3 along the critical line. Although general pattern is the same as for the circle map, there are some noticeable departures.

FIG. 5. Frequency-scaled power spectrum for the excited wake at the critical golden-mean point (to within 0.1%).

ed essentially the same critical line. The nonconstant level of a/D along the critical line for small Ω is not understood, but not surprising considering similar findings in Ref. 7. In Fig. 3 we highlight the fine structure of the phase diagram in a region just below the $\frac{1}{3}$ tongue.

The experimentally determined devil's staircase along the critical line is shown and compared to the predictions for the circle map at $K=1$ in Fig. 4. The symbols represent the limits of the experimental steps, while the solid lines with vertical limiting bars represent predictions. Although a staircase structure is definitely obtained in experiments, the limitation of the agreement between the measured fine structure and the devil's staircase is obvious especially from the inset enlarging the boxed region.

In Fig. 5 we show a typical scaled power spectrum of the wake velocity at the critical golden-mean point shown by the square symbol in Fig. 2. The dressed winding number ω is within 0.1% of σ_G, this being the best control possible in our experiments. The spectrum is averaged over approximately 65000 cycles of the cylinder oscillation frequency. The circle map predicts a self-similar power spectrum (when power is scaled with f^2) divided into bands by the principal sum and difference frequencies located at all powers of σ_G. These peaks are commonly designated as generation-1 peaks. Other generations are created by positive-integer mixing coefficients of various Fibonacci sequences, $f = |j\sigma_G - k|$ — generation 2 by the sequence $(2,2,4,6,...)$, generation 3 by the sequence $(1,3,4,7,...)$, etc; peaks within each generation are of constant amplitude for the circle map. In Fig. 5 we see that the principal peaks fall at powers of σ_G down to σ_G^5. They are nearly of constant amplitude except for σ_G^5 which falls off. We note that the generation-2 and -3 peaks fall as predicted by the
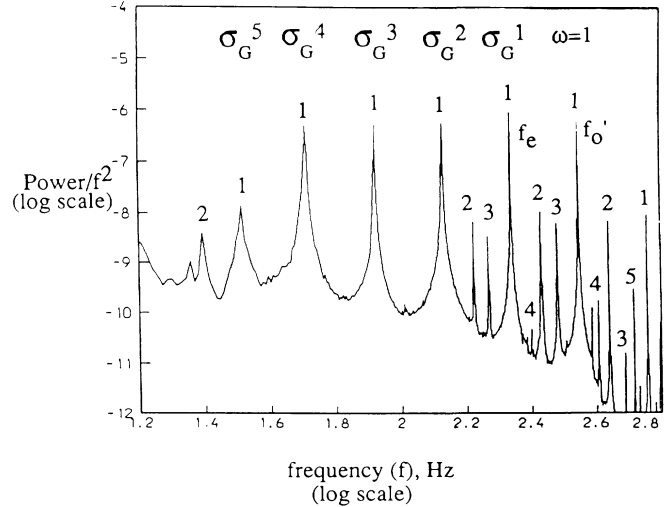
mixing coefficients within the resolution of our power spectrum. We also see that generation-2 peaks show the constant-amplitude trend, but generation-3 peaks and beyond degrade considerably. Generation-2 and -3 peaks are not present at lower frequencies and higher generations are observed rather rarely.

Finally, from the time series of velocity obtained at the critical golden-mean point, we constructed a pseudo attractor by the usual time-delay methods and obtained Poincaré sections by sampling data at intervals separated by the period of forcing. The resulting Poincaré section was embedded in three dimensions (in which it was nonintersecting in all three views), and a smoothed attractor was obtained by performing averages locally. The data were then used to compute the so-called generalized dimensions[18] by using the standard box-counting methods; in each of the appropriate log-log plots, the
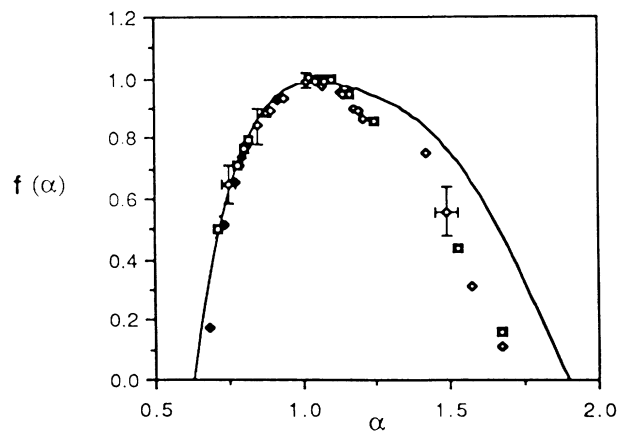

FIG. 6. The $f(\alpha)$ curve obtained via Legendre transform (Ref. 16) of the measured generalized dimensions. Levels of uncertainty are shown by error bars.

scale similarity regime extended typically over two decades. The multifractal spectrum [or the $f(\alpha)$ curve[16]] was then obtained via a Legendre transform discussed in Ref. 16. The result is compared in Fig. 6 with the theoretical curve for the circle map.

Even though some departures from the circle-map behavior do exist, we think that the extent of the observed similarity is remarkable. It is not obvious whether these departures are real, or whether they occur because the control of experimental parameters was not as fine tuned as desired. It is known, however, that very small departures from criticality can produce similar behavior.[19,20] As already noted, inherent difficulties in the establishment of the flow made it impossible to control σ_G to better than 0.1%. The departures observed in the devil's-staircase construction are of the same order of magnitude as the uncertainties in the flow parameters. Further, the largest departures in the $f(\alpha)$ occur for large α, consistent with the relatively large influence of noise on the most sparsely populated (that is, large α) regions of the attractor. Apropos of this somewhat unsatisfactory state of affairs, we reiterate that we exercised enormous care in the experiments, and believe that the residual problems of fine control cannot be eliminated without our resorting to unconventional ways of generating such flows; some thoughts on this are currently being investigated.

[1]M. J. Feigenbaum, J. Stat. Phys. **19**, 25 (1979).

[2]M. J. Feigenbaum, Phys. Lett. **74A**, 375 (1979).

[3]S. J. Shenker, Physica (Amsterdam) **5D**, 405 (1982).

[4]M. J. Feigenbaum, L. P. Kadanoff, and S. J. Shenker, Physica (Amsterdam) **5D**, 370 (1982).

[5]S. Ostlund, D. Rand, J. Sethna, and E. Siggia, Physica (Amsterdam) **8D**, 303 (1983).

[6]D. Rand, S. Ostlund, J. Sethna, and E. Siggia, Phys. Rev. Lett. **49**, 132 (1982).

[7]J. Stavans, F. Heslot, and A. Libchaber, Phys. Rev. Lett. **55**, 596 (1985).

[8]M. H. Jensen, L. P. Kadanoff, A. Libchaber, I. Procaccia, and J. Stavans, Phys. Rev. Lett. **55**, 2798 (1985).

[9]A. P. Fein, M. S. Heutmaker, and J. P. Gollub, Phys. Scr. **T9**, 79 (1985).

[10]K. R. Sreenivasan, in *Frontiers of Fluid Mechanics,* edited by S. H. Davis and J. L. Lumley (Springer-Verlag, Berlin, 1985), p. 41.

[11]K. R. Sreenivasan and R. Ramshankar, Physica (Amsterdam) **23D**, 246 (1986).

[12]K. R. Sreenivasan and P. J. Strykowski, in *Turbulence and Chaotic Phenomena in Fluids,* edited by T. Tatsumi (North-Holland, Amsterdam, 1984), p. 191.

[13]G. Schewe, Phys. Lett. **109A**, 47 (1985).

[14]K. R. Sreenivasan, P. J. Strykowski, and D. J. Olinger, in *American Society for Mechanical Engineers Forum on Unsteady Flow Separation,* edited by K. N. Ghia, Fluids Engineering Division Vol. 52 (American Society for Mechanical Engineers, New York, 1987), p. 1.

[15]M. H. Jensen, P. Bak, and T. Bohr, Phys. Rev. A **30**, 1960 (1984).

[16]T. C. Halsey, M. H. Jensen, L. P. Kadanoff, I. Procaccia, and B. I. Shraiman, Phys. Rev. A **33**, 1141 (1986).

[17]G. H. Koopman, J. Fluid Mech. **28**, 501 (1967).

[18]H. G. E. Hentshel and I. Procaccia, Physica (Amsterdam) **8D**, 435 (1983).

[19]A. Arneodo and M. Holschneider, Phys. Rev. Lett. **58**, 2007 (1987).

[20]J. A. Glazier, G. Gunaratne, and A. Libchaber, Phys. Rev. A **37**, 504 (1988).